American Mineralogist, Volume 89, pages 94–101, 2004

Dehydration dynamics of bikitaite: Part I. In situ synchrotron powder X-ray diffraction study

ORAZIO FERRO,[1,†] SIMONA QUARTIERI,[2] GIOVANNA VEZZALINI,[1,*] CHIARA CERIANI,[3] ETTORE FOIS,[3] ALDO GAMBA,[3] AND GIUSEPPE CRUCIANI[4]

[1]Dipartimento di Scienze della Terra, Largo S. Eufemia, 19, I-41100 Modena, Italy
[2]Dipartimento di Scienze della Terra, Salita Sperone 31, I-98166 Messina-S.Agata, Italy
[3]Dipartimento di Scienze Chimiche, Fisiche e Matematiche, via Lucini 3, I-22100, Como, Italy

ABSTRACT

The thermal dehydration process of the natural Li zeolite bikitaite has been studied in situ by synchrotron radiation powder diffraction. The temperature-resolved experiments were performed using a translating imaging plate system. Rietveld refinements were carried out on 42 powder patterns in the temperature range from room temperature to 800 °C. Bikitaite is stable at least up to 800 °C, the temperature at which the phase transition to γ-spodumene begins. The dehydration process begins at about 200 °C, affecting the two water sites in a similar way, and is complete at 468 °C. Such a process induces only very minor structural distortions in the framework, due to the anti-rotation of the internal T-O-T hinges. In this sense, bikitaite can be defined as a flexible but non-collapsible framework, and it is the zeolite that undergoes the lowest heating-induced distortion among those studied up to now. The high thermal and structural stability suggest that anhydrous bikitaite could be used as a solid porous matrix for embedding nanosized materials in its one-dimensional channels.

INTRODUCTION

Bikitaite [$Li_2(Al_2Si_4O_{12})\cdot 2H_2O$, space group = $P1$] is a rare Li zeolite, characterized by the highest framework density among the minerals of this family. Its structure, also observed in the synthetic alumino-silicate $Cs_{0.35}Al_{0.35}Si_{2.65}O_6$ (Annehed and Fälth 1984), can be described as sheets of 6-membered rings, parallel to the ***a-b*** plane, connected to each other by pyroxene-like chains developing along ***b***. Non-crossing channels, delimited by 8-membered rings, run along the same direction and host Li^+ cations, which are tetrahedrally coordinated to three framework O atoms and one water molecule. The peculiarity of this zeolite is due to the presence of water molecules, hydrogen bonded to each other to form a one-dimensional chain, parallel to the channel direction, defined as "one-dimensional ice" because of the absence of hydrogen bonds with the framework (Ståhl et al. 1989; Quartieri et al. 1999). This "floating" water system is stabilized by host-guest interactions based on the antiparallel dipole moments of framework and water chains (Fois et al. 1999).

Confinement of materials in ordered matrices is, at present, of primary interest for applied research. In fact, it is known that a low-dimensional system has different properties from the ones of the corresponding bulk material, which can be of relevance for the tailoring of new materials (Czapleswky et al. 2002; Fois et al. 2001a; Mac Dougall et al. 1989; Vietze et al. 1998). Bikitaite is a good example of confinement of a low-dimensionality system in an ordered matrix (Fois et al. 2001b, 2001c). To understand how low-dimensional species can be inserted and stabilized in materials like zeolites, it is essential to study the stability of this system under different physico-chemical conditions. In this respect, the behavior of bikitaite under high pressure has recently been described by Ferro et al. (2002) using an experimental-computational approach. Here, we will present the results of the study on the thermal stability and dehydration mechanism of this zeolite.

The knowledge of the thermal behavior of zeolites and of the structural modifications induced by dehydration is of particular importance, owing to the wide application of these materials. For this reason, thermal behavior has been widely and systematically studied by many authors; in particular it has been schematized by Alberti and Vezzalini (1984) and reviewed by Ståhl (1994), Artioli (1999), and Bish and Carey (2001).

Kocman et al. (1974) and Phinney and Stewart (1961) studied the thermal behavior of bikitaite by thermogravimetry in air, observing a continuous water loss between 150 and 400 °C. Rehydration was complete up to 240 °C, nearly complete after heating between 240 and 360 °C, scarce between 360 and 600 °C. Rapid heating in air above 750 °C decomposed the zeolite to form β-spodumene or β-eucryptite (Phinney and Stewart 1961). Hurlbut (1957) observed the transformation of bikitaite to β-spodumene upon heating to 900 °C.

Bikitaite belongs to the mordenite group, which also includes ferrierite, dachiardite, and epistilbite. All these zeolites are characterized by the presence of columns of 5-membered tetrahedral rings. This structural feature strongly contributes to the high thermal stability of these phases (Breck 1974).

The present investigation considers the structural response of bikitaite to temperature-induced dehydration, and was carried out using in situ temperature-resolved powder X-ray diffraction (XRD) with synchrotron radiation. This technique allows rapid collection of diffraction data so as to follow in detail each dehydration step; moreover these powder patterns can be used

* E-mail: giovanna@unimo.it
† Deceased 28 February 2003.

for full-profile Rietveld structural analysis yielding a continuous picture of the structure during dehydration. However, this experimental approach is not suited to the detailed position refinement of very light elements—like Li—or for studying the dynamical evolution of the hydrogen bonding system. Hence, we adopted an integrated experimental-theoretical approach based on both synchrotron XRD and ab initio molecular dynamics simulations, which provided the complementary results presented in part I and II, respectively, of this paper.

Experimental section

The bikitaite sample used in this work is from Bikita, Zimbabwe. The cell parameters determined at room T (rT) are a= 8.606(1), b = 4.9573(4), c = 7.5970(7), α = 89.94(6), β = 114.407(9), γ = 89.98 (5). The assumed space group was $P1$, on the basis of the structural refinements performed on samples from Bikita (Bissert and Liebau 1986; Ståhl et al. 1989) and from North Carolina (Quartieri et al. 1999), respectively.

The thermal analysis was performed in air, on about 27 mg of sample, using a Seiko SSC/5200 instrument operating at a heating rate of 4.7 °C/min from rT to 1000 °C (Fig. 1).

Data collection

The temperature-resolved XRD experiments were performed at the GILDA beam line operating at the European Synchrotron Radiation Facilities (Grenoble, France). The powdered sample of bikitaite was carefully packed inside a 0.3 mm capillary open at both ends. Two different cycles of diffraction experiments (henceforth called experiment A and B) were carried out under different experimental conditions. In both cycles of experiments, data was acquired in parallel Debye-Scherrer geometry. In experiment A, with LaB_6 refined wavelength of 0.95337(1) Å, the rotating capillary sample was heated in situ by means of hot air stream equipment with a heating rate of 4.7 °C/min, from rT up to 800 °C. The XRD patterns were collected continuously during the entire heating process on the 4 mm slit-delimited slice of a translating image-plate detector (Norby 1997; Meneghini et al. 2001) located at a sample-to-detector distance of 204.2 mm in order to obtain a resolution, sin θ/λ, up to 0.484/Å. A total of 81 powder patterns were extracted by integrating temperature slices of 10 °C width and separation between subsequent integration intervals of 10 °C.

For experiment B, a ramp-and-pause mode was chosen on the basis of the results obtained from the Rietveld refinements performed previously (experiment A), and will be dealt with in the refinement and discussion sections below. Using the same equipment and a new LaB_6 refined wavelength of 1.04022(1) Å, three data collections were carried out in the temperature interval: rT-280, 280–700, and 700–800 °C. In all these intervals, the XRD patterns were collected continuously on 2.5 mm delimited-slit slice of a translating image plate, with a sample-to-detector distance of 288.5 mm and a heating rate of 4 °C/min. Moreover, three additional full-screen isothermal patterns also were collected at 280, 700, and 800 °C, namely the extremes of the intervals reported above. Full-screen patterns on the image-plate detector offer the advantages of more statistics and higher resolution profiles with respect to the patterns collected on the translating detector, as the integration is carried out on a pie slice of about 36 degrees from full sections of diffraction cones. However, the $\sin\theta/\lambda$ resolution 0.3679 is the same, both in the full-screen isothermal patterns and in the slit-delimited slice patterns. A further additional isothermal pattern was collected after 30 min cooling of the sample, in order to study a possible reversibility of the dehydration process.

The criterion for data extraction "by slices" on the scanning of the three image plates, relative to the three heating intervals, was the same used previously in experiment A, with the difference that for the same slice width in pixels, different temperature widths occur depending on the different reported temperature intervals; namely the applied integration slice of 25 pixels corresponds to 3.45, 5.70, and 1.41 °C width for rT – 280, 280–700 and 700–800 °C intervals, respectively.

To study the thermal stability and the phase transition of bikitaite beyond 800 °C (maximum temperature reachable with the heating system mounted at GILDA beamline), an in situ time-resolved powder XRD experiment with a conventional source was performed with a continuous heating ramp up to 1000 °C (experiment C), using a Siemens D5000 instrument with Bragg-Brentano θ–2θ geometry and a position sensitive detector (Fig. 2).

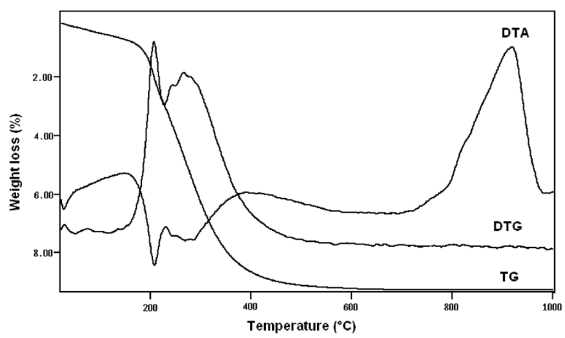

Figure 1. Thermogravimetric curves for bikitaite.

Rietveld refinement

The GSAS package (Larson and Von Dreele 1994) was used for Rietveld profile fitting. Structure refinements were performed in the $P1$ space group. The refinement of the first pattern collected was started using the atomic coordinates reported in Quartieri et al. (1999).

Experiment A. The extracted Bragg peak profiles were modeled by a pseudo-Voight function with 3 refined coefficients (Gw, Lx, Ly) and a 0.01% cut-off of the peak intensity. The background curve was fitted with a 22 refined coefficient Chebyshev polynomial. The refined structural parameters included: the fractional coordinates and isotropic thermal displacement parameters of all atoms, and the occupancy factors for water molecules. Soft-constraints were applied initially to the T-O distances and then gradually relaxed after the initial stages of refinement. The thermal displacement parameters were constrained in the following way: the same value for all Si atoms, another for all Al atoms, and a third for the two Li cations. Three different thermal parameters were assumed, respectively, for the framework O atoms bounded to Li1, for those bounded to Li2, and for the six O atoms non-bounded to any extra-framework cations. This choice was suggested by the values of the independently refined thermal parameters reported in Quartieri et al. (1999) and Ståhl et al. (1989) as a result of single-crystal experiments. Concerning the isotropic thermal parameters of water molecules, our choice pointed to a non-constrained option, in order to find—cycle after cycle throughout the dehydration process—reliable values of both water occupancy factors and thermal parameters. However, in the final steps of water site depopulation, at about 420 °C, the same thermal motion for both independent water sites was imposed.

With increasing temperature, an abnormal increase of the Gw coefficient of the pseudo-Voight function was observed and, at about 320 °C, a peak doubling for all the profile lines appeared. This feature became more and more evident with increasing temperature, and at about 700 °C the split reached is maximum. Since the unit cell of bikitaite is pseudo-monoclinic, the hkl and $\bar{h}k\bar{l}$ reflections occur at very close 2θ positions, and at rT they overlap in unique peaks. The new peaks deriving from their splitting could easily be indexed and interpreted as due

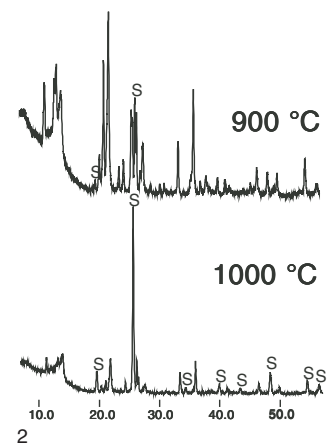

Figure 2. Powder XRD patterns of bikitaite at 900 and 1000 °C (experiment C). The peaks labeled S belong to the new phase γ-spodumene.

to a larger deviation from the pseudo-monoclinicity. However, this interpretation is not correct, as the doubling of the reflections belonging to the *h0l* group is not justifiable by the same argument. After the unsuccessful efforts to find possible superstructures, we concluded in favor of the hypothesis of the co-existence of two lattice distortions related to two distinct, but similar, evolutions of the system under these heating conditions. Because the lattice parameters and the structural information derived by the Rietveld refinements of the split system were unreliable above 400 °C, we performed an additional dehydration experiment under the different heating conditions above described (experiment B).

Experiment B. Refinement strategies for experiment B were the same used for experiment A. In the patterns of experiment B, however, no abnormal increase of Gw occurred and the disturbing splitting phenomena of h0l reflections were not observed. Hence, reliable lattice parameters (Fig. 3) and structural information were obtained by refinements up to 800 °C. The final observed and calculated powder patterns for bikitaite at selected temperatures are reported in Figure 4. Table 1 reports the unit-cell and the Rietveld refinement parameters for bikitaite structure at 30, 280 (full screen isothermal pattern), 400, and 468 °C. The refined atomic coordinates, isotropic thermal parameters, and water molecule occupancies are given in Table 2.

In spite of the low Li diffraction power and the high temperatures, some peaks in the Fourier difference map were observed up to 470 °C and refined as Li positions.

Results and discussion

Thermal gravimetrical analysis

The TG curve (Fig. 1) shows a slight slope variation below 200 °C, which can be ascribed to the loss of surface humidity. The main water loss occurs between 200 and 500 °C, whereas above this temperature a further small and slow water loss is observed up to about 800 °C. The total weight loss is hence 9.1%. In the *T* range 200–400 °C, DTG and DTA curves show a narrow low-*T* and a broader high-*T* peak. These features suggest a two-step dehydration behavior, which will be discussed in the following section and interpreted in detail in Part II of this work. In addition, the DTA curve (Fig. 1) shows a strong exothermic peak between 800 and 1000 °C that is ascribed, as discussed in the next section, to the phase transition of bikitaite to γ-spodumene.

To test the reversible dehydration capacity of bikitaite, 13.116 mg of powder were heated to 200, 400, 500, 600, 700, and 800 °C and cooled each time to r*T* in air for 24 hours before re-heating. The rehydration is scarce between 200 and 800 °C, whereas after heating at 800 °C no water regain is observed.

Powder patterns were collected on the anhydrous phase obtained from a continuous TG experiment, one immediately after heating, and another after one year of sample exposure to air. The comparison of the peak intensities of the two powder patterns reveals the stability of anhydrous bikitaite and the irreversibility of the dehydration process over this period of time. This conclusion was confirmed by the absence of maxima ascribable to water molecules in the difference Fourier map obtained by the structural refinement of the sample left in air for one year.

Table 1. Experimental and refinement parameters for bikitaite at selected temperatures

T (°C)	30	280	400	468
a (Å)	8.6121(2)	8.6140(2)	8.6269(2)	8.6274(2)
b (Å)	4.9579(1)	4.9721(1)	4.9871(1)	4.9898(1)
c (Å)	7.6040(2)	7.5510(2)	7.5718(2)	7.5729(2)
α (°)	89.892(3)	89.753(2)	89.765(3)	89.737(3)
β (°)	114.423(1)	114.273(1)	114.097(1)	114.072(1)
γ (°)	89.955(3)	90.154(2)	90.160(2)	90.169(2)
V (Å³)	295.62(1)	294.81(1)	297.38(1)	297.65(1)
R_p(%)	6.4	5.2	6.6	6.7
R_{wp}(%)	8.9	8.0	8.9	9.1
R_F^2	10.6	11.1	16.1	13.1
Reduced χ^2	39.1	29.3	30.3	30.9
No. of variables	106	104	106	97
No. of observations	3985	4020	4061	4009
No. of reflections	292	292	299	291

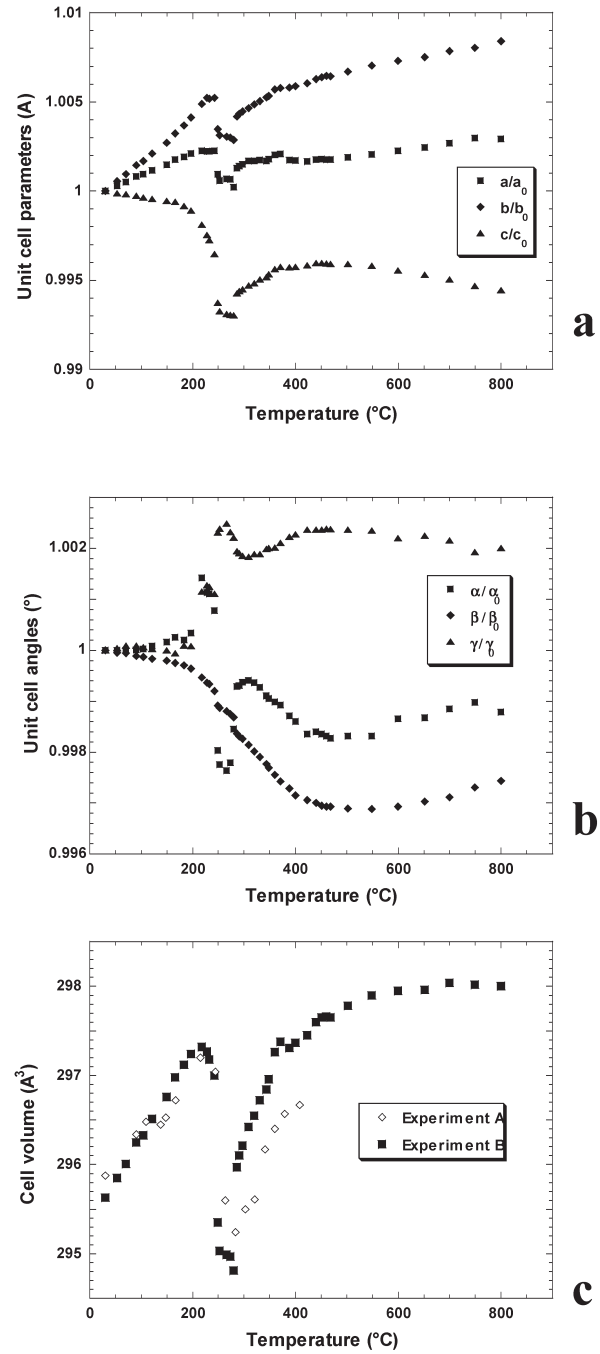

Figure 3. Temperature dependence of the unit-cell axes (**a**) and angles (**b**) from experiment B, and volumes (**c**) from experiments A and B.

Table 2. Fractional coordinates, thermal parameters and occupancies for bikitaite at selected temperatures

Atom	x	y	z	U_{iso}	x	y	z	U_{iso}
	***T*= 30 °C**				***T*= 280 °C**			
Si11	0.086(2)	0.871(3)	0.100(2)	3.7(2)	0.092(2)	0.863(3)	0.080(2)	2.2(2)
Si12	0.1038	0.8006	0.5049	3.7(2)	0.1038	0.8006	0.5049	2.2(2)
Al13	0.373(2)	0.896(3)	0.942(2)	3.0(3)	0.376(2)	0.876(3)	0.924(2)	1.2(3)
Al21	0.880(2)	0.392(4)	0.910(3)	3.0(3)	0.883(2)	0.376(3)	0.896(2)	1.2(3)
Si22	0.885(2)	0.324(4)	0.491(2)	3.7(2)	0.886(1)	0.321(3)	0.487(2)	2.2(2)
Si23	0.607(2)	0.385(3)	0.068(2)	3.7(2)	0.6120(2)	0.363(3)	0.059(2)	2.2(2)
O11	0.256(3)	0.787(5)	0.068(4)	3.1(6)	0.251(3)	0.756(4)	0.038(3)	2.1(5)
O12	0.049(3)	0.184(4)	0.035(4)	3.1(6)	0.063(3)	0.180(3)	0.021(3)	2.1(5)
O13	0.152(4)	0.848(6)	0.328(3)	3.1(3)	0.134(3)	0.834(6)	0.309(2)	2.4(3)
O14	0.055(3)	0.496(3)	0.526(4)	3.1(3)	0.051(2)	0.513(3)	0.561(3)	2.4(3)
O15	0.261(3)	0.933(5)	0.690(3)	3.1(3)	0.252(2)	0.952(4)	0.684(2)	2.4(3)
O16	0.423(3)	0.228(4)	0.020(4)	3.1(6)	0.437(3)	0.195(4)	0.018(4)	2.1(5)
O21	0.714(3)	0.240(5)	0.958(4)	2.3(5)	0.728(3)	0.237(4)	0.960(4)	2.9(6)
O22	0.899(3)	0.732(4)	0.963(4)	2.3(5)	0.912(3)	0.720(3)	0.943(3)	2.9(6)
O23	0.828(4)	0.345(6)	0.667(3)	3.1(3)	0.806(3)	0.352(5)	0.646(2)	2.4(3)
O24	0.953(3)	0.020(5)	0.475(5)	3.1(3)	0.961(3)	0.019(4)	0.497(4)	2.4(3)
O25	0.738(3)	0.432(6)	0.292(3)	3.1(3)	0.715(2)	0.368(5)	0.292(2)	2.4(3)
O26	0.543(3)	0.678(4)	0.973(4)	2.3(5)	0.554(3)	0.667(4)	0.980(4)	2.9(6)
Li1	0.270(3)	0.395(5)	0.128(5)	4.5(14)	0.286(3)	0.374(4)	0.128(4)	8.3(16)
Li2	0.659(3)	0.876(5)	0.831(4)	4.5(14)	0.674(3)	0.871(4)	0.843(4)	8.3(16)
O17*	0.412(4)	0.366(7)	0.413(4)	3.0(6)	0.398(6)	0.277(11)	0.411(5)	14(1)
O27†	0.583(4)	0.849(6)	0.541(4)	3.0(6)	0.542(6)	0.810(10)	0.558(4)	14(1)
	***T*= 400 °C**				***T*= 468 °C**			
Si11	0.102(2)	0.851(4)	0.078(2)	5.6(3)	0.105(3)	0.866(3)	0.090(2)	4.5(2)
Si12	0.1038	0.8006	0.5049	5.6(3)	0.1038	0.8006	0.5049	4.5(2)
Al13	0.384(2)	0.859(4)	0.933(2)	3.6(3)	0.377(2)	0.874(4)	0.931(3)	4.1(4)
Al21	0.889(2)	0.336(4)	0.899(2)	3.6(3)	0.891(3)	0.357(4)	0.895(3)	4.1(4)
Si22	0.883(2)	0.292(3)	0.484(2)	5.6(3)	0.886(2)	0.313(4)	0.494(2)	4.5(2)
Si23	0.617(2)	0.334(4)	0.074(3)	5.6(3)	0.618(2)	0.367(4)	0.068(3)	4.5(2)
O11	0.246(3)	0.706(5)	0.020(4)	4.6(6)	0.264(3)	0.727(5)	0.055(4)	4.3(6)
O12	0.085(3)	0.179(4)	0.029(4)	4.6(6)	0.083(3)	0.191(4)	0.039(4)	4.3(6)
O13	0.124(4)	0.819(7)	0.301(3)	5.0(4)	0.135(4)	0.808(7)	0.310(3)	5.0(3)
O14	0.024(3)	0.522(3)	0.538(4)	5.0(4)	0.044(3)	0.520(3)	0.559(4)	5.0(3)
O15	0.266(2)	0.882(6)	0.695(3)	5.0(4)	0.267(3)	0.914(5)	0.687(3)	5.0(3)
O16	0.436(3)	0.188(5)	0.014(4)	4.6(6)	0.445(3)	0.190(5)	0.018(4)	4.3(6)
O21	0.723(3)	0.242(5)	0.951(4)	4.2(6)	0.738(3)	0.246(5)	0.972(4)	4.6(6)
O22	0.936(3)	0.673(4)	0.952(4)	4.2(6)	0.938(3)	0.684(4)	0.972(4)	4.6(6)
O23	0.813(3)	0.343(7)	0.650(3)	5.0(4)	0.795(3)	0.326(6)	0.644(3)	5.0(3)
O24	0.946(3)	0.985(4)	0.489(5)	5.0(4)	0.954(3)	0.012(5)	0.479(5)	5.0(3)
O25	0.736(3)	0.419(5)	0.296(3)	5.0(4)	0.721(3)	0.380(6)	0.299(3)	5.0(3)
O26	0.550(3)	0.629(5)	0.975(4)	4.2(6)	0.559(3)	0.673(5)	0.997(4)	4.6(6)
Li1	0.314(4)	0.356(6)	0.160(4)	7.1(17)	0.320(4)	0.352(5)	0.167(5)	7.2(18)
Li2	0.718(4)	0.844(5)	0.914(8)	7.1(17)	0.718(4)	0.859(5)	0.911(8)	7.2(18)
O17*	0.526(8)	0.333(24)	0.416(8)	15(5)				
O27†	0.633(10)	0.793(19)	0.625(8)	15(5)				

* Occupancy factors at 30, 280, and 400 °C respectively: 1.0, 0.66(5), 0.36(4).
† Occupancy factors at 30, 280, and 400 °C respectively: 1.0, 0.77(5), 0.41(5).

Phase transition

Figure 2 shows the powder patterns of bikitaite heated at 900 and 1000 °C (Experiment C). It is evident that bikitaite is still present up to 1000 °C; however, between 900 and 1000 °C, a new phase, labeled **s**, appears in the patterns. This new phase was identified as the $LiAlSi_2O_6$ III polymorph (or γ-spodumene) (Li 1968). This result is apparently in disagreement with that obtained by Hurlbut (1957) and Phinney and Stewart (1961), who reported the decomposition of bikitaite to different anhydrous phases (ß- spodumene or β-eucryptite). However, as discussed by Li (1968), this is due to the confusion present in the literature regarding the nomenclature of the anhydrous phases with composition $LiAlSi_2O_6$.

The temperature at which γ-spodumene appears is strongly dependent on the kinetics of the dehydration process. In fact, in experiments A and C, and during the thermal analysis—all conducted with continuous heating—we did not observe the phase transition up to 900 °C. In contrast, during experiment B, carried out by the ramp-and-pause mode, γ-spodumene already appears at 800 °C. As expected, this result suggests that a slower heating kinetics favors the phase transition.

The cell parameters of γ-spodumene were refined, together with those of bikitaite, from the powder pattern collected at 800 °C during experiment B, and are the following: $a = b = 5.222(1)$ Å, $c = 5.432(2)$ Å, $V = 128.29(6)$ Å^3. These parameters are in good agreement with those reported by Li (1968) for the hexagonal $LiAlSi_2O_6$ III polymorph and are equal—within the experimental error bars—to those obtained on our sample cooled and kept for 30 min at r*T*.

Temperature-dependent variation of unit-cell parameters

The main difference between the results of experiments A and B, carried out with different heating ramps, is the progressive peak broadening followed by a splitting at about 330 °C of the reflections in experiment A, as discussed above in the section on Rietveld refinement. This split, which prevented the structural refinement, could be due to two different distortion paths, which drive the system toward geometrically slightly different,

but energetically similar, distorted unit cells. This phenomenon also was observed in experiment C and in the powder patterns collected on the sample used for the TG analysis, immediately after heating and after one year of sample exposure to air. In contrast, the split was not observed during experiment B, conducted with the ramp-and-pause mode and, hence, in the following, all the structural considerations will be based on the results of experiment B.

A careful analysis of the powder patterns reveals that, in the temperature range r*T*-800 °C, no phase transition occurs and only slight variations in the peak positions and intensities are observed.

Figure 3 shows the variations of the unit-cell axes, angles, and volume, as a function of temperature. It is evident, at first glance, that bikitaite is very rigid almost undeformable under dehydration: the *T*-induced variations are in fact only 0.27, 0.85, –0.64, –0.03, –0.24, 0.24, 0.70% for *a*, *b*, *c*, α, β, γ and *V*, respectively. However, in spite of these very small variations, almost all the cell parameters undergo an abrupt increase or decrease in the first stages of the dehydration process, between 200 and 300 °C. In particular, at about 280 °C, *a*, *b*, *c*, α, and *V* show minimum values, whereas γ shows a maximum. Before and after this *T* range, we instead observe much smoother variations. The β angle shows a sinusoidal trend in the complete *T* range. In general, the variation of α and γ angle distortions indicates that the structure becomes slightly more triclinic.

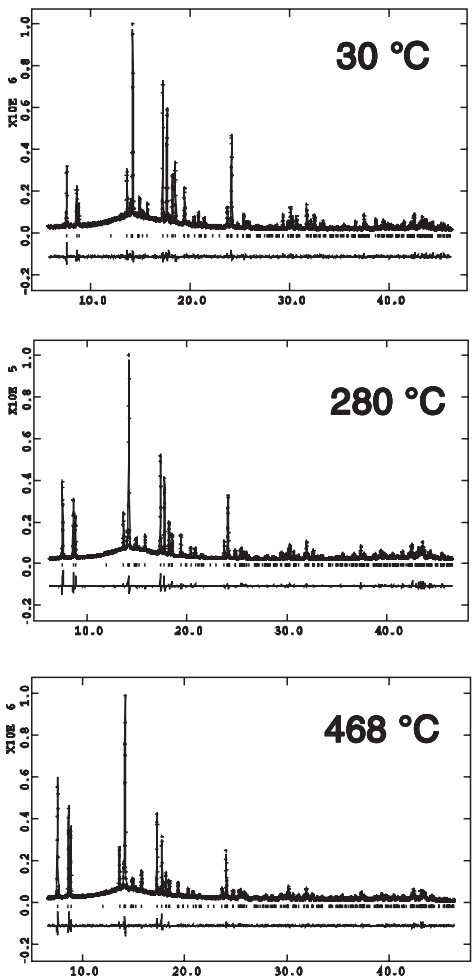

Figure 4. Observed (dotted line) and calculated (continuous line) XRD patterns and final difference curve from Rietveld refinements of bikitaite at 30, 280 (full-screen isothermal pattern), and 468 °C.

Crystal structure modifications upon dehydration

Extraframework species. Figure 5 reports the *T*-dependence of the refined occupancies of the two water sites labeled O17 and O27, and of the water content as measured by TG analysis. Dehydration affects the two water sites in a similar way, even if the water loss of the O17 site is always slightly advanced with respect to that of O27. The differences between the dehydration temperatures estimated by XRD and TG analyses can be ascribed to the different amount and arrangement of the powder in the sample holders used in the two experiments.

The water system of bikitaite has been widely investigated by different techniques, both experimental (Larsson et al. 1989; Ståhl et al. 1989; Quartieri et al. 1999; Kolesov and Geiger 2002) and computational (Fois et al. 1999, 2001b, 2001c). The similar thermal behavior of the two water molecules is completely justifiable on the basis of their similar crystallographic environments. Moreover, water release is accompanied by an increase of the water O atom atomic displacement parameters and a slight lengthening of O17-O27 bond distance that, at the end, induces the breaking of the "floating" one-dimensional water chains hosted in the bikitaite channels. As a consequence, in the structure refinements of the powder patterns collected above 270 °C, we observe the approach of the water molecules toward framework O atoms; at different temperatures the framework atoms involved in these interactions are different. The formation of these new water-framework interactions should modify the water release mechanism and, hence, explain the two peaks observed in the DTG and DTA curves in the 200–400 °C temperature range (Fig. 1).

Due to the difficulties and limits of the Rietveld refinements

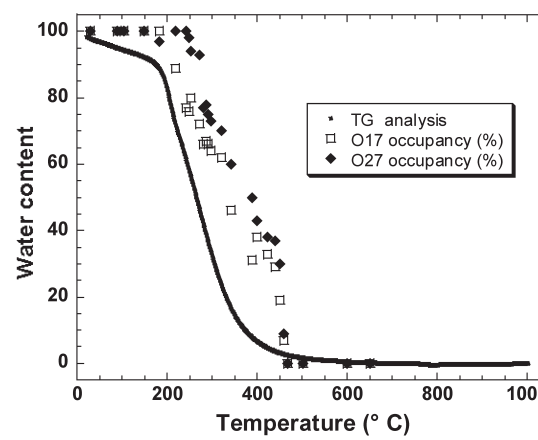

Figure 5. Comparison of the water content variation with temperature as calculated from the refined occupancies determined by experiment B (O17: open squares; O27 filled diamonds), and as measured by the TG analysis (solid line).

of light elements, especially on the basis of in situ high-*T* XRD patterns, the detailed study of the thermal effects on the water system was tackled by a computational approach, and the discussion of these results is reported in the companion paper (part II) of this work. Here, we simply anticipate that also in the simulations of bikitaite containing less than 100% water, weak interactions between water and framework O atoms are observed.

For the same reasons reported above for water molecules, the detailed discussion of the *T*-induced modifications of the Li coordination polyhedron can be found in part II. From an experimental point of view, we observe a decrease of Li coordination number from 4 to 3 upon complete water loss. The unusual threefold coordination of lithium also has been found in KLiO (Sabrowsky et al. 1985), in the dehydrated LiNa-A zeolite (Jirák et al. 1983) and, very recently, in $LiBaB_9O_{15}$ (Pushcharovsky et al. 2002).

Before complete dehydration, the partial water loss induces a slight shift of Li2 (above 343 °C) toward the channel walls and a distortion of the internal angles of the Li coordination tetrahedra. These geometrical modifications are accompanied by a very slight shortening of the Li-O bond distances—generally within the experimental error bars (see Table 3).

Framework. Figures 6 and 7 show the projections along *b* and *c* of the bikitaite structure, that is, the 8-ring channels and the hexagonal sheets, at selected temperatures. As indicated by the behavior of the unit-cell parameters and the T-O bond distances reported in Table 3, the bikitaite framework undergoes only very small distortions. In particular, the channels running along *b* are non-squeezable upon dehydration, as a consequence of the anti-rotation (that is the distortion in an opposite sense) of the couples of internal T-O-T angles centered on O23 and O13, O25 and O15, and O21 and O11. The modifications of these angles only allow a slight pear-like distortion of the channels with increasing temperature.

The layer of 6-membered rings seems to be relatively more flexible upon dehydration. The two crystallographically independent ditrigonal rings are labeled 1 and 2 in Figure 7, the former being slightly smaller than the latter at r*T*. Upon water loss, ring 1 enlarges while ring 2 becomes smaller, and at about 400 °C their sizes invert and ring 1 becomes significantly larger than ring 2. Also the internal O-O-O angles of the 6-membered rings undergo modifications with *T*, inducing a less ditrigonal shape in the rings up to about 400 °C. Above this *T*, upon complete water loss, the original geometry of the layer is restored and all these distortions are resolved.

Finally, the pyroxene-like chain becomes less corrugated in both ***a-b*** and ***b-c*** planes, and its internal O24-O14-O24 angle tends to increase in the studied *T* range. This behavior is related to the increase of the *b* parameter.

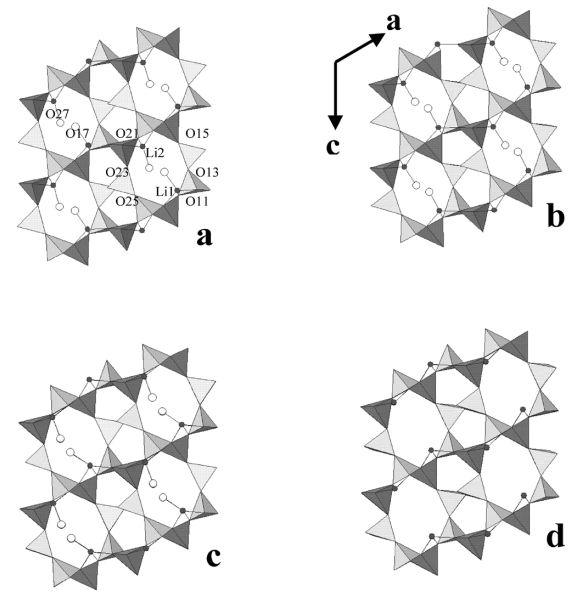

FIGURE 6. Projections along *b* axis of bikitaite structure at (**a**) 30, (**b**) 280, (**c**) 400, and (**d**) 468 °C.

TABLE 3. T-O and Li-O distances (Å) for bikitaite at selected temperatures

	Temperature (°C)					Temperature (°C)			
	30	280	400	468		30	280	400	468
Si11-O11	1.64(1)	1.628(5)	1.64(1)	1.65(1)	Si12-O13	1.58(1)	1.615(5)	1.63(1)	1.60(1)
Si11-O12	1.62(1)	1.627(5)	1.67(1)	1.66(1)	Si12-O14	1.60(1)	1.607(5)	1.61(1)	1.60(1)
Si11-O13	1.59(1)	1.617(5)	1.62(1)	1.61(1)	Si12-O15	1.64(1)	1.614(5)	1.60(1)	1.62(1)
Si11-O22	1.67(1)	1.630(5)	1.62(1)	1.63(1)	Si12-O24	1.64(1)	1.623(5)	1.61(1)	1.62(1)
T-O mean	1.63	1.625	1.64	1.64	T-O mean	1.61	1.615	1.61	1.61
Al13-O11	1.74(1)	1.733(7)	1.75(1)	1.76(1)	Al21-O12	1.71(1)	1.749(7)	1.76(1)	1.77(1)
Al13-O15	1.76(1)	1.721(7)	1.67(1)	1.71(1)	Al21-O21	1.78(1)	1.736(7)	1.70(1)	1.74(1)
Al13-O16	1.74(1)	1.732(7)	1.74(1)	1.72(1)	Al21-O22	1.72(1)	1.746(7)	1.74(1)	1.72(1)
Al13-O26	1.75(1)	1.751(7)	1.76(1)	1.76(1)	Al21-O23	1.73(1)	1.732(7)	1.73(1)	1.74(1)
T-O mean	1.75	1.734	1.73	1.74	T-O mean	1.73	1.741	1.73	1.74
Si22-O14	1.62(1)	1.608(5)	1.60(1)	1.61(1)	Si23-O16	1.66(1)	1.620(5)	1.60(1)	1.62(1)
Si22-O23	1.61(1)	1.618(5)	1.62(1)	1.62(1)	Si23-O21	1.64(1)	1.620(5)	1.62(1)	1.62(1)
Si22-O24	1.64(1)	1.625(5)	1.62(1)	1.64(1)	Si23-O25	1.62(1)	1.614(5)	1.63(1)	1.61(1)
Si22-O25	1.61(1)	1.617(5)	1.60(1)	1.61(1)	Si23-O26	1.61(1)	1.624(5)	1.64(1)	1.63(1)
T-O mean	1.62	1.617	1.61	1.62	T-O mean	1.63	1.619	1.62	1.62
Li1-O11	1.99(2)	1.996(7)	2.00(2)	2.03(2)	Li2-O21	2.01(2)	1.993(7)	2.01(2)	1.98(2)
Li1-O12	2.03(2)	2.001(7)	2.01(2)	2.04(2)	Li2-O22	2.02(2)	2.015(7)	1.98(2)	1.97(2)
Li1-O16	2.00(2)	2.015(7)	2.00(2)	2.03(2)	Li2-O26	2.00(2)	2.006(7)	2.00(2)	1.97(2)
Li1-O17	2.00(2)	2.004(7)	2.05(2)	—	Li2-O17	2.03(2)	2.005(7)	2.02(2)	—

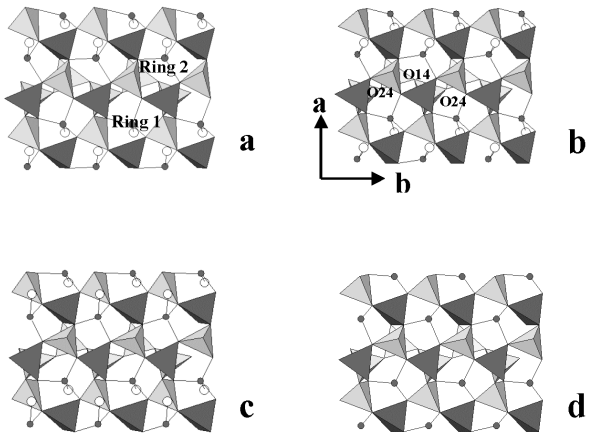

FIGURE 7. Projections along *c* axis of bikitaite structure at (**a**) 30, (**b**) 280, (**c**) 400, and (**d**) 468 °C.

CONCLUDING REMARKS

A poor thermal stability could be predicted for bikitaite simply by considering the very low Si/Al ratio, a factor that is known to affect the structural stability of zeolites adversely upon dehydration (Smith 1976; Bish and Carey 2001). In contrast, bikitaite is very stable up to at least 800 °C, the temperature at which the phase transition to γ-spodumene starts. This stability can be attributed to the presence of columns of 5-membered tetrahedral rings in the bikitaite framework, as in mordenite and ferrierite (all belonging to the mordenite group), which possess one of the highest levels of thermal stability (Breck 1974).

In contrast to the dehydration behavior reported for all the other zeolites, bikitaite undergoes an overall, even if very small, cell volume increase, with an anomalous and irregular trend (Fig. 3c). In the ranges r*T* to 200 °C and 280 to 700 °C, the small volume increase can be explained by the thermal expansion. This effect is usually not appreciable during zeolite heating, because it is masked by the high volume decrease generally induced by water loss in these minerals. In contrast, the *T*-induced volume decrease in bikitaite, from the beginning of dehydration to the minimum at about 280 °C, is extremely limited (0.8%), due to the anti-rotating behavior of the internal T-O-T hinges. Following Baur (1992a, 1992b; 1995), the zeolite frameworks can be defined as flexible or inflexible following changes of the physico-chemical conditions. The flexible structures are classified as collapsible or non-collapsible; in collapsible frameworks the T-O-T hinges co-rotate, while in the non-collapsible ones the hinges anti-rotate, preventing cell volume changes. Hence, bikitaite can be defined as a flexible but non-collapsible framework, and it is the zeolite that undergoes the lowest heating-induced distortion upon dehydration among those that have been studied.

Considering its demonstrated high thermal and geometrical stability, anhydrous bikitaite could be a good candidate for use as a solid porous matrix in the fabrication of nanosized materials confined in its one-dimensional channel system. In addition, as discussed in detail in part II of this work, the embedded nanomaterial would possibly be stabilized by host-guest interactions with the bikitaite framework, based on its high permanent dipole moment, in particular after draining off water molecules.

ACKNOWLEDGMENTS

This paper is dedicated to Orazio Ferro, who died prematurely at age 33. He was deeply involved in this research and made a large contribution to the present paper. The authors are indebted to Daniele Malferrari and Eugenia Marchi for the thermal analysis and to Edoardo Mazzucato for the XRD data collection of experiment C. The European Synchrotron Radiation Facility is kindly acknowledged for allocation of beam-time under proposals CH545 and GILDA 08-02-267. This work was supported by Italian MIUR (COFIN2001 "Le zeoliti, materiali di interesse per l'industria e l'ambiente: sintesi, struttura, stabilità e applicazioni." and FIRB2002 "Proprietà ed applicazioni tecnologiche di minerali e loro analoghi di sintesi").

REFERENCES CITED

Alberti, A. and Vezzalini, G. (1984) Topological changes in dehydrated zeolites: breaking of T-O-T oxygen bridges. In D. Olson and A. Bisio, Eds., Proceedings of the 6th International Zeolite Conference, 834–841. Reno. Butterworth, Guildford, U.K.

Annehed, H. and Fälth, L. (1984) The crystal structure of $Cs_{0.35}Al_{0.35}Si_{2.65}O_6$, a cesium-aluminosilicate with the bikitaite framework. Zeitschrift für Kristallographie, 166, 301–306.

Artioli, G. (1999) In-situ structural and kinetic powder diffraction studies of aluminosilicates. In K. Wright and R. Catlow, Eds., Microscopic properties and processes in minerals, NATO Science Series, Series C, 543, 177–187. Kluwer, Dordrecht.

Baur, W.H. (1992a) Why the open framework of zeolite A does not collapse, while the dense framework of natrolite is collapsible. In M. Rozwadowski, Ed., Proceedings of Polish-German Zeolite Colloquium, Nicholas Copernicus University Press, Torun, 11–19.

——— (1992b) Self-limiting distorsion by antirotating hinges of flexible but non-collapsible frameworks. Journal of Solid State Chemistry, 97, 243–247.

——— (1995) Framework mechanics: limits to the collapse of tetrahedral framework. Proceedings 2nd Polish-German Zeolite Colloquium. M. Rozwadowski Ed., Nicholas Copernicus University Press, Torun, 171–185.

Bish, D.L. and Carey J. W. (2001) Thermal behavior of natural zeolites. In D.L. Bish, D.W. Ming, Eds., Natural zeolites: occurrence, properties, applications, 45, 403–452. Reviews in Mineralogy and Geochemistry, Mineralogical Society of America, Washington, D.C.

Bissert, G. and Liebau, F.N. (1986) The crystal structure of a triclinic bikitaite, $Li[AlSi_2O_6] \cdot H_2O$, with ordered Al/Si distribution. Neues Jahrbuch für Mineralogie Monatshefte, H6, 241–252.

Breck, D.W. (1974) Zeolite Molecular Sieves. Wiley, New York.

Czapleswky, K.F., Reitz, T.L., Kim, Y.J., and Snurr R.Q. (2002) One-dimensional zeolites as hydrocarbon traps. Microporous and Mesoporous Materials, 41, 55–64.

Ferro, O., Quartieri, S., Vezzalini, G., Fois, E., Gamba, A., and Tabacchi, G. (2002) High-pressure behaviour of bikitaite: an integrated theoretical and experimental approach. American Mineralogist, 87, 1415–1425.

Fois, E., Tabacchi, G., Quartieri, S., and Vezzalini, G. (1999) Dipolar host/guest interactions and geometrical confinement at the basis of the stability of one-dimensional ice in zeolite bikitaite. Journal of Chemical Physics, 111, 355–359.

Fois, E., Gamba, A., and Spanò, E. (2001a) Electronic properties of new zeolitic supra-lattices. Physical Chemistry Chemical Physics, 3,1877–1882.

Fois, E., Gamba, A., Tabacchi, G., Quartieri, S., and Vezzalini, G. (2001b) Water molecules in single file: first-principles studies of one-dimensional water chains in zeolites. Journal of Physical Chemistry B, 105, 3012–3016.

——— (2001c) On the collective properties of water molecules in one-dimensional zeolitic channels. Physical Chemistry Chemical Physics, 3, 4158–4163.

Hurlbut, C.S. (1957) Bikitaite, a new mineral from Southern Rhodesia. American Mineralogist, 42, 792–797.

Jirák, Z., Bosacek, V., Vratislav, S., Herden, H., Schöllner, R., Mortier, W.J., Gellens, L., and Uytterhoeven, J.B. (1983) Crystal structure of dehydrated LiNa-A type zeolites. Zeolites, 3, 255–258.

Kocman, V., Gait, R.I., and Rucklidge, J. (1974) The crystal structure of bikitaite. American Mineralogist, 59, 71–78.

Kolesov, B.A. and Geiger, C.A. (2002) Raman spectroscopic study of H_2O in bikitaite: "One- dimensional ice". American Mineralogist, 87, 1426–1431.

Larson, A.C. and Von Dreele, R.B. (1994) GSAS-General Structure Analysis System. Report LAUR 86-748, Los Alamos National Laboratory, Los Alamos, New Mexico.

Larsson, K., Tegenfeldt, J., and Kvick, Å. (1989) NMR study of the motion of water molecules in the natural zeolite bikitaite. Journal of Physics and Chemistry of Solids, 50, 107–110.

Li, C.T. (1968) The crystal structure of $LiAlSi_2O_6$ III (high-quartz solid solution). Zeitschrift für Kristallographie, 127, 327–348.

MacDougall, J.E., Eckert, H., Stucky, G.D., Herron, N., Wang, Y., Moller, K., Bein, T., and Cox, D. (1989) Synthesis and Characterization of III-V Semiconductor Cluster: GaP in zeolite Y. Journal of American Chemical Society, 111, 8006–8007.

Meneghini, C., Artioli, G., Balerna, A., Gualtieri, A.F., Norby, P., and Mobilio, S. (2001) Multipurpose imaging-plate camera for in-situ powder XRD at the GILDA beamline. Journal of Synchrotron Radiation, 8, 1162–1166.
Norby, P. (1997) Synchrotron powder diffraction using imaging plates: crystal structure determination and Rietveld refinement. Journal of Applied Crystallography, 30, 21–30.
Phinney, W.C. and Stewart, D.B. (1961) Some physical properties of bikitaite and its dehydration and decomposition products. US Geological Survey Professional Paper, 424, 353–357.
Pushcharovsky, D. Yu., Gobetchia, E. R., Pasero, M., Merlino, S., and Dimitrova, O.V. (2002) Hydrothermal synthesis and crystal structures of Li,Ba-nanoborate, LiBaB9O15, and Ba- borophosphate, BaBPO5. Journal of Alloys and Compounds, 339, 70–75.
Quartieri, S., Sani, A., Vezzalini, G., Galli, E., Fois, E., Gamba, A., and Tabacchi, G. (1999) One-dimensional ice in bikitaite: single-crystal X-ray diffraction, infra-red spectroscopy and ab initio molecular dynamics studies. Microporous and Mesoporous Materials, 30, 77–87.
Sabrowsky, H., Mertens, P., and Thimm, A. (1985) KLiO: Ein Oxid mit dreifach koordiniertem Lithium. Zeitschrift für Kristallographie, 171, 1–6.
Smith, J.V. (1976) Origin and structure of zeolites. In J.A. Rabo, Ed., Zeolite Chemistry and Catalysis, 171, 1–79. ACS Monograph, Washington, D.C.
Ståhl, K. (1994) Real-time powder diffraction studies of zeolites dehydration processes. Materials Science Forum, 166–169, 571–576.
Ståhl, K., Kvick, Å., and Ghose, S. (1989) One-dimensional water chain in the zeolite bikitaite: neutron diffraction study at 13 and 295K. Zeolites, 9, 303–311.
Vietze, U., Krauss, O., Laeri, F., Ihlein, G., Schüth, F., Limburg, B., and Abraham, M. (1998) Zeolite-Dye Microlasers. Physics Review Letters, 81, 4628–4631.

Manuscript received February 10, 2003
Manuscript accepted June 9, 2003
Manuscript handled by Alison Pawley